In this section, the challenges and limitations of using cross-polarization suppression methods for dual-linear polarization antenna arrays are presented. A simple probe-fed patch antenna and a high-performance, high isolation, low cross-polarization dual-polarized patch antenna are used for this study. The image feed method is used for improving the cross-polarization level and increasing the geometrical symmetry of the large array antenna. It is shown that decomposing the antenna radiation pattern to its even and odd components for calculating 2×2-element subarray radiation pattern has fundamental limitations and none of four different 2×2-element subarray configurations will totally suppress the sidelobe issue of configured arrays. The accuracy of using embedded element pattern for calculating the radiation pattern of the large array with identical subarrays is studied and an accurate procedure for predicting array antenna radiation pattern is proposed. The appearance of undesired sidelobes has been studied, and an optimal design for the large array of 2×2-element subarrays with image configuration is presented to avoid the sidelobes.

According to **woelder1997cross**, the radiation pattern of an array antenna which is made of the 2×2-element subarrays can be calculated by separating the single element radiation pattern to its even and odd components. The main concern about the provided results in **woelder1997cross** is that the all calculations are based on the isolated element pattern which is obtained from measuring the radiation pattern of a single probe-fed patch antenna on a 0.75 m × 0.75 m ground plane. First, the radiation pattern of an element in an array is different from the isolated element pattern. To better predict the array radiation pattern, the embedded element pattern which contains the coupling effects of the adjacent element should be utilized. The embedded element pattern is defined as the radiation pattern of the center element in the array of unique elements. However, in the 2×2-element subarray, the array elements are mirrored, and the relative location of H and V ports are changed, leading the change of the radiation pattern. Consequently, calculation of the radiation pattern of an array of similar 2×2-element subarrays becomes a complicated problem.

The full-wave method can be used for simulation of small array antennas, however, this problem for the large antenna arrays, which cannot be simulated by using full-wave methods, is more severe. The decomposition approach and the results presented in **woelder1997cross** will be discussed in this paper and it is shown that the calculated radiation patterns of the 2×2-element subarray based on the measured or simulated radiation pattern of a single element are not accurate enough. In this paper, it is shown that the sidelobe level suppression by using configuration ?D?, is generally based on calculation error and undesired sidelobes still exist.

This paper is organized as follows: In section II, issues of cross-polarization suppression in dual-polarization array antennas using the even and odd decomposition method is discussed. In section III, the coupling effect is discussed and the method of calculating the radiation pattern of the array of identical subarrays with image arrangement presented in **woelder1997cross** is introduced, and the radiation pattern of different 2×2-element subarrays with image configuration are compared. In section IV, the limitations of using image configuration are illustrated and discussed in detail, and the solution and optimum design for a large phased array antenna are presented in section V. Finally, the summary is provided at the end of the paper.

Figure 1: $2 \times 2$-element subarray configuration for cross-polarization suppression. The ports marked with ”-” are excited with a 180° phase shift with respect ports marked with ”+” **saeidi2017characterization**.

## 0.1 Issues with even and odd component decomposition method

A well-known method for cross-polarization suppression in dual-polarized array antennas is image arrangement in which elements are arranged into the group of $2 \times 2$-element subarrays **woelder1997cross**, **saeidi2017cross**. Fig. **??** shows four different forms of $2 \times 2$-element subarrays in which either horizontal ports or vertical ports or both are mirrored regarding horizontal and vertical planes. The mirrored ports will be excited with 180°phase shift, so the mirrored elements copolarization radiation patterns will be in-phase, and cross-polarization radiation patterns will be 180° out of phase compared to the reference element in the subarray. This will result in cross-polarization suppression especially in principle planes. Based on simulation and measurement results in **woelder1997cross**, using image configuration will result in cross-polarization suppression, however, it could cause undesired side lobes if configuration ”B” or ”C” is used. Based on calculated results in **woelder1997cross** the cross-polarization and side lobe level suppression is possible by using configuration ”D”. The cross-polarization suppression by using image configuration has been studied in different articles, and presented results show that the configuration ”D” has the best performance. However, configuration ”C” provides more geometrical symmetry which makes this configuration an exciting choice if the side lobe issue can be avoided.

The calculated radiation patterns of configuration ”B”, ”C”, and ”D” in **woelder1997cross** are based on the measured radiation pattern of a single isolated probe-fed patch antenna. To calculate the radiation pattern of the $2 \times 2$-element subarray, the single element horizontal and vertical polarizations co and cross-polarization patterns are decomposed to their even and odd components. Then the radiation pattern of other mirrored elements in the subarray is calculated based on the separated even and odd components, the excitation phase, and relative location of H and V ports. There are two main concerns about the results calculated with this approach. First, in this method, the isolated element radiation pattern is used which doesn't contain the coupling effect of the other elements. The second issue with calculated radiation patterns using this method is that since the elements in the $2 \times 2$-element subarray are not identical and the adjacent elements of each element of the $2 \times 2$-element subarray have different orientation, one element pattern regardless of being isolated element pattern or embedded element pattern, cannot be used for calculating the radiation pattern of the embedded $2 \times 2$-element subarray. This means that the calculated results in **woelder1997cross** are not generally true. To prove this claim, the radiation pattern of a $2 \times 34$-element array of a probe-fed patch antenna configured according to configuration "D" is calculated using two methods. The first method is based on separating the single element pattern to its even and odd component and then calculating the $2 \times 2$-element array radiation pattern. The second method is based on a full-wave simulation result which is a perfectly acceptable approach.

Assuming the antenna is placed in the x-y plane and antenna boresight is in the z-direction the even and odd component of the antenna radiation pattern would be:

$$\begin{aligned} E^{even}_{H,V}(\theta,\varphi) &= \tfrac{E_{H,V}(\theta,\varphi)+E_{H,V}(-\theta,\varphi)}{2} \\ E^{odd}_{H,V}(\theta,\varphi) &= \tfrac{E_{H,V}(\theta,\varphi)-E_{H,V}(-\theta,\varphi)}{2} \end{aligned} \tag{1}$$

And following the same procedure in **woelder1997cross**, the radiation pattern of the upper left $E_L(\theta,\varphi)$ and right $E_R(\theta,\varphi)$ elements in the $2\times2$-element subarray can be written as follows:

$$E_L(\theta,\varphi) = \begin{Bmatrix} E^{h}_{E}(\theta,\varphi) = E^{he}_{E}(\theta,\varphi) + E^{ho}_{E}(\theta,\varphi) \\ E^{v}_{E}(\theta,\varphi) = E^{ve}_{E}(\theta,\varphi) + E^{vo}_{E}(\theta,\varphi) \end{Bmatrix} \tag{2}$$

$$E_R(\theta,\varphi) = \begin{Bmatrix} E^{h}_{E}(\theta,\varphi) = -E^{he}_{E}(\theta,\varphi) + E^{ho}_{E}(\theta,\varphi) \\ E^{v}_{E}(\theta,\varphi) = \quad E^{ve}_{E}(\theta,\varphi) - E^{vo}_{E}(\theta,\varphi) \end{Bmatrix} \tag{3}$$

In which $E^{he}_{E}(\theta,\varphi)$ and $E^{ho}_{E}(\theta,\varphi)$ are the even and odd components of horizontal polarization radiation pattern and $E^{ve}_{E}(\theta,\varphi)$ and $E^{vo}_{E}(\theta,\varphi)$ are the even and odd components of the vertical polarization radiation pattern.

The radiation pattern of upper two elements of the subarray with configuration ”D” can be written as follows:

$$\begin{aligned} E^{H}_{2\times1,U}(\theta,\varphi) &= \frac{1}{\sqrt{2}}\left(e^{-j\beta}E^{H}_{L}(\theta,\varphi) - e^{j\beta}E^{H}_{R}(\theta,\varphi)\right) \\ &= \sqrt{2}\begin{Bmatrix} \cos BE^{Hhe}_{E}(\theta,\varphi) - j\sin BE^{Hho}_{E}(\theta,\varphi) \\ -j\sin BE^{Hve}_{E}(\theta,\varphi) + \cos BE^{Hvo}_{E}(\theta,\varphi) \end{Bmatrix} \end{aligned} \tag{4}$$

$$
\begin{aligned}
E^{V}_{2\times 1,U}(\theta,\varphi) &= \frac{1}{\sqrt{2}}\left(e^{-j\beta}E^{V}_{L}(\theta,\varphi)+e^{j\beta}E^{V}_{R}(\theta,\varphi)\right)\\
&= \sqrt{2}\begin{Bmatrix} -j\sin BE^{Vhe}_{E}(\theta,\varphi)+\cos BE^{Vho}_{E}(\theta,\varphi)\\ \cos BE^{Vve}_{E}(\theta,\varphi)-j\sin BE^{Vvo}_{E}(\theta,\varphi)\end{Bmatrix}
\end{aligned} \tag{5}
$$

In which $B = \frac{k_0 d_x}{2}\cos(\varphi)\sin(\theta)$ and $d_x$ is the spacing between elements along x-axis and $k_0$ is the wavenumber. The radiation pattern of lower two elements can be calculated by reversing the $B$ sign in equation (**??**) and (**??**) as follows:

$$
\begin{aligned}
&E^{H}_{2\times 1,L}(\theta,\varphi)\\
&\qquad= \sqrt{2}\begin{Bmatrix} \cos BE^{Hhe}_{E}(\theta,\varphi)+j\sin BE^{Hho}_{E}(\theta,\varphi)\\ j\sin BE^{Hve}_{E}(\theta,\varphi)+\cos BE^{Hvo}_{E}(\theta,\varphi)\end{Bmatrix}
\end{aligned} \tag{6}
$$

$$
\begin{aligned}
&E^{V}_{2\times 1,L}(\theta,\varphi)\\
&\qquad= \sqrt{2}\begin{Bmatrix} j\sin BE^{Vhe}_{E}(\theta,\varphi)+\cos BE^{Vho}_{E}(\theta,\varphi)\\ \cos BE^{Vve}_{E}(\theta,\varphi)+j\sin BE^{Vvo}_{E}(\theta,\varphi)\end{Bmatrix}
\end{aligned} \tag{7}
$$

The radiation pattern of the $2\times 2$-element subarray can be calculated based on the radiation pattern of the two upper and lower elements:

$$
E_{2\times 2}(\theta,\varphi) = \frac{1}{\sqrt{2}}\left(e^{-jC}E_{2\times 1,L}(\theta,\varphi)+e^{jC}E_{2\times 1,U}(\theta,\varphi)\right) \tag{8}
$$

In which $C = \frac{k_0 d_y}{2}\sin(\varphi)\sin(\theta)$ and $d_y$ is the spacing between elements along y-axis. After substituting (**??**) and (**??**) in (**??**) and simplifying the results, the radiation pattern of the $2\times 2$-element array antenna with configuration "D" in $\varphi = 0°$ and $\varphi = 90°$ planes can be written as:

$$
E^{H}_{2\times 2,D}(\theta,0) = 2\begin{Bmatrix} \cos BE^{Hhe}_{E}(\theta,0)\\ \cos BE^{Hvo}_{E}(\theta,0)\end{Bmatrix} \tag{9}
$$

$$E^{V}_{2\times 2,D}(\theta,0) = 2\begin{Bmatrix} \cos BE^{Vho}_{E}(\theta,0) \\ \cos BE^{Vve}_{E}(\theta,0) \end{Bmatrix} \tag{10}$$

$$E^{H}_{2\times 2,D}(\theta,\pi/2) = 2\begin{Bmatrix} \cos CE^{Hhe}_{E}(\theta,\pi/2) \\ \cos CE^{Hvo}_{E}(\theta,\pi/2) \end{Bmatrix} \tag{11}$$

$$E^{V}_{2\times 2,D}(\theta,\pi/2) = 2\begin{Bmatrix} \cos CE^{Vho}_{E}(\theta,\pi/2) \\ \cos CE^{Vve}_{E}(\theta,\pi/2) \end{Bmatrix} \tag{12}$$

For a fair comparison, the radiation pattern of a similar probe-fed patch antenna at 2.8 GHz is used for calculating the radiation pattern of $2\times2$-element subarray array with configuration "D".

The radiation pattern of the $N \times M$-element array of subarray can be calculated as follows:

$$E_{2N\times 2M}(\theta,\varphi) = AF_{N\times M}(\theta,\varphi) \times AF_{2\times 2}(\theta,\varphi) \times E(\theta,\varphi) \tag{13}$$

In which the $AF_{N\times M}(\theta,\varphi)$ is the array factor of the array of subarrays, $AF_{2\times 2}(\theta,\varphi)$ is the array factor of the $2 \times 2$-element array, and $E_{2N\times 2M}(\theta,\varphi)$ is the radiation pattern of the $N \times M$-element array of subarrays.

The radiation patterns of the $2\times2$-element subarray and the $1\times17$-element array of the subarray are presented in Fig. **??**. As seen in Fig. **??**, similar to the results presented in **woelder1997cross** there is no sidelobe in the array radiation pattern for both horizontal and vertical polarization in $\varphi = 90°$ plane.

As mentioned before, this method of analysis along with using a single isolated element pattern does not consider the coupling between elements. To verify the accuracy of the radiation patterns calculated using the decomposition method, a $1\times17$-element array of a $2\times2$-element subarray of the probe-fed

Chapters/Ch6_Figs/PIC/New/even_odd_of_D1.pdf

(a)

Chapters/Ch6_Figs/PIC/New/even_odd_of_D2.pdf

(b)

Figure 2: $2 \times 2$-element subarray and $2 \times 34$-element array radiation pattern calculated using decomposition method in $\varphi = 90°$ plane; (a) H-pol; (b) V-pol.

patch antenna is simulated using HFSS. As shown in Fig. **??**, a pair of the sidelobes appeared for both polarizations in $\varphi = 90°$ plane. The sidelobe level for horizontal and vertical polarizations is -21 dB and -32 dB, respectively. Clearly, the appearance of the undesired sidelobe cannot be predicted by the decomposition method. Therefore, the calculated results in **woelder1997cross** and decomposition method, depending on the single element design, may not be generally true. Also, from the measured radiation pattern of the $8 \times 2$-element antenna with configuration ”D” in **woelder1997cross**, it can be seen that the undesired sidelobes will appear. The sidelobe level in measured radiation pattern has been related to the small ground plane, however, as it is shown here, the sidelobes exist even if configuration ?”D”? is implemented. It should be mentioned that simulation results show the level of undesired sidelobes depends on the single element design. The reason for the appearance of the sidelobes will be discussed in the next section.

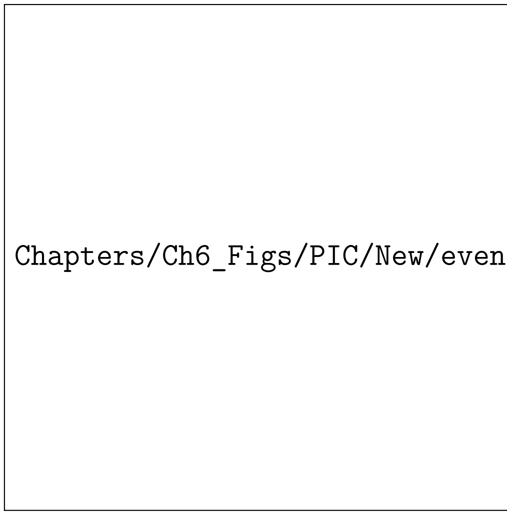

(a)

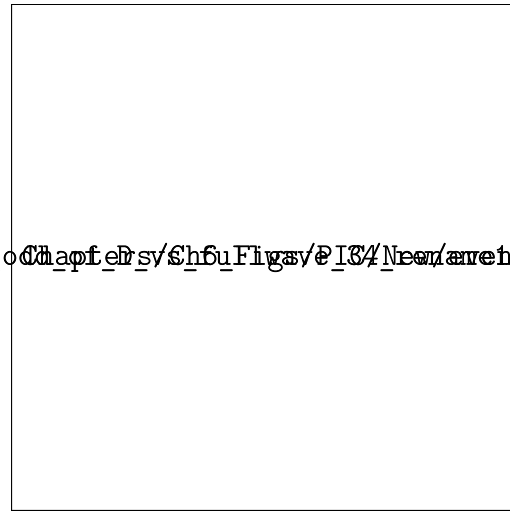

(b)

Figure 3: $2 \times 2$-element subarray and $2 \times 34$-element array radiation pattern calculated using decomposition method and full-wave simulations in $\varphi = 90°$ plane; (a) H-pol; (b) V-pol.

## 0.2 Coupling Effect and Method of Calculation

It is seen from the previous section that the calculated radiation pattern of the array of subarray using decomposition method while the adjacent element coupling effect is neglected leads to inaccurate results. The coupling associated with elements in the array of identical subarrays is emanating from two facts. The first fact is the existence of adjacent elements and the second is the orientation of the surrounding elements. To investigate the effect of the orientation of the elements on the coupling between elements and final array radiation pattern, first, the embedded element radiation pattern of the array of identical elements is calculated by full-wave simulation. To calculate the embedded element pattern, the radiation pattern of the center element in a $7 \times 7$-element array is simulated while all other elements are terminated. In this case, the orientation of the elements is neglected. The radiation pattern of the $2 \times 2$-element pattern with configuration ”D” is then calculated by decompo-

(a) (b)

Figure 4: $2 \times 2$-element subarray and $2 \times 34$-element array radiation pattern calculated using decomposition method and identical array embedded element pattern; (a) H-pol; (b) V-pol.

sition method. Using (**??**), the radiation pattern of the $2 \times 34$-element array is calculated. As seen in Fig. **??** including the coupling between elements, changes the $2 \times 34$-element pattern but cannot predict the side lobes.

To characterize the effects of element orientation on the subarray radiation pattern, the $2 \times 2$-element subarrays with different configurations are simulated using HFSS. Fig. **??**, show the radiation pattern of the isolated $2 \times 2$-element array of a probe-fed patch antenna with configuration ”A” (no image configuration), ”C”, and ”D”, with the H-pol and V-pol excitations. The element spacing (d) in these simulations is 55 mm. In $\varphi = 0°$ and $\varphi = 90°$ planes, using image configuration, especially configuration ”C”, will significantly improve the cross-polarization level of the $2 \times 2$-element array. Also, not shown here, in the $\varphi = 45°$ plane, image configuration has improved the cross-polarization level in the main beam area. As shown in Fig. **??** the copolarization radiation patterns in all three arrays are almost laid on each other, and there is no degradation in a copolarization radiation pattern of $2 \times 2$-element array compared to the radiation pattern of the array with configuration ”A”.

Clearly, applying the array factor of an array of the subarrays will result in similar copolarization patterns for all three configurations. In other words, any calculated radiation pattern of larger arrays based on the isolated $2 \times 2$-element subarray pattern is not accurate enough for predicting the undesired side lobe precisely.

For further explanation, the array factor of a large array ($2 \times 34$-element array) of the probe-fed patch antenna is calculated by different methods. The array factor of the $2N \times 2M$-element array is the combination of the array factor of the $2 \times 2$-element array and $N \times M$-element array antenna which is shown in Fig. **??**. As is shown in Fig. **??**, the grating lobe of $N \times M$-element array antenna (with an inter-element spacing of 110 mm) appears in $\theta = 77°$. On the other hand, the first null of the array factor $2 \times 2$-element array (with an inter-element spacing of 55 mm) is precisely at the location of the grating lobe of $N \times M$-element array. Consequently, based on equation (**??**), the effect of the peak of the array factor of $N \times M$-element array in total array radiation pattern will be eliminated with the null of the array factor $2 \times 2$-element array. As shown in Fig. **??**, there is no grating lobe or undesired side lobe in the array factor of the $2N \times 2M$-element array.

The radiation pattern of a $2 \times 34$-element array of the probe-fed patch antenna with configuration ”A” is calculated using two different methods. In the first method, the array factor of the $2 \times 2$-element array is applied on the isolated element pattern to calculate the radiation pattern of the $2 \times 2$-element array antenna. The array factor of the $1 \times 17$-element array antenna is then applied on the calculated $2 \times 2$-element array radiation pattern to calculate the $2 \times 34$-element array radiation pattern. In the second method, the $2 \times 2$-element array radiation pattern is calculated using the full-wave simulations and then the array factor of the $1 \times 17$-element array antenna is applied. As shown in Fig. **??** and Fig. **??** (a), the radiation pattern of the $2 \times 2$-element array antenna calculated with the two methods are similar in the main beam area. It can be seen that the sharp null of the array factor of the $2 \times 2$-element array exists in the radiation pattern calculated based the first method, however, in the full wave results, there is no null. The importance of the null in $2 \times 2$-element array radiation pattern is described in Fig. **??** as it eliminates the grating lobe peak of the array factor of $N \times M$-element array (spacing = 2d). When the null is removed from $2 \times 2$-element array radiation pattern the effect of the grating lobe of the $N \times M$-element array will show up in the $2N \times 2M$-element array radiation pattern.

Fig. **??** (b) and Fig. **??** (b) show the radiation pattern of the $2 \times 34$-element array. As shown in Fig. **??** (b), the effect of the grating lobe of the array factor of the $1 \times 17$-element array antenna appears in the results calculated with method 2. The $2 \times 2$-element array radiation pattern and the final array radiation pattern for the vertical polarization are shown in Fig. **??**. As shown in Fig. **??** (a), for the vertical polarization, compared to the horizontal polarization, the full wave results of the $2 \times 2$-element array radiation pattern is closer to the results calculated with applying the array factor $2 \times 2$-element array. Consequently, the side lobes with the lower peak are expected. Fig. **??** (b) shows the vertical polarization radiation pattern of the $2 \times 34$-element array. As shown in Fig. **??** (b), the local grating lobe still exists but with reduced peak power compared to horizontal polarization results. Comparing the two calculated radiation patterns shows that the using isolated $2 \times 2$-element array pattern leads to inaccurate results. This means that the coupling caused by the existence of the adjacent elements and the effect of elements orientation cannot be separated.

## 0.3 Embedded Subarray Pattern and Limitations of Image Configuration

Full-wave simulations can be used for predicting the radiation pattern of small array antennas. However, for large array antennas, alternative solutions should be utilized. The embedded element pattern is the radiation pattern of the central element in an array while all other elements are terminated. The embedded subarray pattern could be defined as the radiation pattern of the central subarray in the array of the subarrays, while all the other subarrays are terminated. The radiation pattern of the embedded $2 \times 2$-element subarrays is studied in this section. To calculate the embedded subarray pattern, a $3 \times 3$-element array of the $2 \times 2$-element subarrays is simulated. As shown in Fig. **??** (a), the embedded subarray pattern compared to the ideal $2 \times 2$-element pattern, which is calculated by applying the array factor of the $2 \times 2$-element array to the single element pattern, is missing two symmetric nulls. The effect of these symmetric Nulls on the array radiation pattern was discussed in the Fig. **??**. Consequently, as seen in Fig. **??** (b), the undesired sidelobes appear in the calculated radiation pattern of the $2 \times 34$-element array. Compared to full-wave simulation result which does not have the sidelobes issue, it can be concluded that the calculated embedded subarray pattern of the $6 \times 6$-element array is not accurate enough for predicting the large array radiation pattern.

The reason for the discrepancy between the two radiation patterns is illustrated in Fig. **??**. As shown in Fig. **??** (a), the embedded subarray radiation pattern is highly sensitive to the to the size of the array which is used for calculating the subarray radiation pattern. Based on the simulation results in Fig. **??** (a), as the size of the array increases, the sharper nulls appear in the $2 \times 2$-element subarray array radiation pattern. The null in the embedded subarray radiation pattern appears if the two adjacent elements radiation patterns have the same amplitude and but be 180°out of phase at a certain location. If the number of the element on the right side and left side of each element in the $2 \times 2$-element subarray are different, the conditions for having a perfect null are not met. As the number of the elements increases the ratio of the number of the element on the right side to left side becomes closer to one and subsequently, the depth of the null gets closer to the ideal $2 \times 2$-element array pattern. Fig. **??** (b), shows the radiation pattern of the $2 \times 34$-element array, calculated based on different embedded subarray patterns. As it was expected from embedded subarray patterns, the calculated $2 \times 34$-element array pattern sidelobe level gets closer to the full wave results. The number of array elements for less than 2 dB difference between full-wave and simulation results, using this probe-fed patch antenna, is 18.

## 0.4 Approaches to Design High-Performance Array Antennas

The radiation pattern $2 \times 34$-element array of a probe-fed patch antenna with configuration "C" and "D" is calculated by using the embedded subarray patterns and full wave method. As shown in Fig. **??** and Fig. **??**, the embedded subarray pattern of the 18-element array perfectly predicts the side lobe level issue in configuration "D". This means that on the contrary to claim in **woelder1997cross**, the side lobe issue cannot be solved using configuration

”D”.

Using configuration ”C” and ”D” will significantly improve the cross-polarization level of the array of the probe-fed patch antenna. However, for a dual-polarized phased array antenna, it is always desired to use a high-performance single element which provides high input-isolation between horizontal and vertical polarizations. High performance dual-polarized hybrid feed antennas **wong2002broadband**, **sun2009c**, **saeidi2017hybrid** could be an ideal choice for multifunction applications **saeidi2018high**. Therefore, in this section, a high-performance hybrid feed patch antenna is used as the unit cell for designing a large array antenna.

It is worth noting that the side lobe level associated with each configuration also depends on the geometry of the unit cell. As the element becomes more geometrically symmetric, it will have a more symmetrical radiation pattern. In other words, as the radiation pattern of the element is more symmetric the effect of mirroring the elements on its radiation pattern becomes less visible. An alternative solution for reducing the sidelobe level of the array is decreasing the peak power of the grating lobe of the array of subarrays. The array factors of the array of identical subarrays with different element spacings are shown in Fig. **??**. As shown in Fig. **??**, decreasing the spacing between elements will reduce the peak level of the grating lobe of the identical subarrays. Reducing the subarray spacing from 110 mm to 104 mm and 102 mm will reduce the level of the undesired grating lobes of the array factor of the subarrays for -11 dB and -14 dB, respectively.

For Multifunction Phased Array Radar (MPAR) application the size of the array antenna could be as large as WSR-88D radar. WSR-88D is utilizing an 8.85 m reflector antenna **zhang2011polarimetric**. Considering the Cylindrical Phased Array Radar (CPPAR) and 55 mm spacing between elements, this will lead to a large cylindrical array antenna with approximately more than 130 elements along its axis. For weather application, it is essential for an array antenna to have a symmetrical copolarization and low cross-polarization level radiation pattern. Also achieving the low sidelobe levels in the final array radiation pattern is critical. To achieve a symmetrical radiation pattern with low cross-polarization level, configuration ”C” is an interesting choice because of its symmetrical subarray geometry. According to the aforementioned information and results, the following procedure is being proposed for designing a large phased array antenna and an accurate prediction of the sidelobe level or reducing it to minimum possible level:

1. Designing a single element with maximum possible geometrical and electrical symmetry.

2. Choosing the subarray configuration; configuration ”C” provides more geometrical symmetry, however, configuration ”D? has lower sidelobe level.

3. Extracting the embedded subarray radiation pattern by simulation a large (15 elements or more) linear array of the selected subarray.

4. Calculating the large array radiation pattern using the simulated embedded subarray pattern.

5. Evaluating the sidelobe level of the large array.

6. If the sidelobe level is not as low as the desired level the symmetry of the single element needs to be increased or, the spacing between elements should be decreased.

Following this procedure, the embedded subarray radiation pattern is calculated from the simulation of $2\times34$-element array with configuration "C" and 55 mm interelement spacing. The radiation pattern of the $2\times130$-antenna is then calculated based on the simulated embedded subarray pattern. As shown in Fig. **??**, in a $2\times130$-element array antenna with 55 mm spacing between elements, the level of the undesired local grating lobe is -37 dB. Assuming that the preferred level is -45 dB, the undesired grating lobe level needs to be reduced.

The radiation pattern of the $2\times130$-element and $2\times136$-element array of hybrid feed patch antenna with configuration "C", for different element spacing, are shown in Fig. **??** and Fig. **??**. As shown in Fig. **??** (a), for horizontal polarization with 104 mm subarray spacing, the undesired sidelobe peak is reduced to -47 dB. For vertical polarization as shown in Fig. **??** (b), with 104 mm spacing between subarrays, there is almost no sign of undesired sidelobes. As shown in Fig. **??**, the advantage of decreasing the spacing between elements is in reducing the peak level of the undesired local grating lobes. However, reducing the spacing between elements will increase the coupling between elements which may result in deformation of the radiation pattern of the phased array antenna especially when the beam is steered to off broadside directions. The other disadvantage of decreasing the spacing between elements is increasing the number of required elements which will result in higher cost of fabrication.

To study the effect of reducing the array element spacing, the radiation pattern of the array at the maximum required steering angle for MPAR application which is 20° ($\theta_0 = 20°$) in the elevation direction and in an arbitrary scan angle ($\theta_0 = 45°$) are shown in Fig. **??**. The horizontal polarization and vertical polarization radiation pattern of the array antenna are shown in Fig. **??**(a) and Fig. **??** (b), respectively. The simulation results show no degradation in antenna radiation pattern while the array spacing is reduced to 52 mm and the side lobe level is lower than -40 dB. Therefore, in this design, the optimal spacing between array elements with configuration ”C” for CPPAR in MPAR application would be 52 mm.

Chapters/Ch6_Figs/PIC/NEW/HV_pol_Pin_2x2_isolatedn.pdf

Figure 5: Simulated radiation pattern of the $2 \times 2$-element array of probe-fed patch antenna configured according to the configuration A, C, and D; (a) H-pol, $\varphi = 0°$ plane; (b) H-pol, $\varphi = 90°$ plane; (c) V-pol, $\varphi = 0°$ plane; (d) V-pol, $\varphi = 90°$ plane.

Chapters/Ch6_Figs/PIC/New/Array_factor_location_N_M1.pdf

(a)

Chapters/Ch6_Figs/PIC/New/Array_factor_locatio

(b)

Figure 6: (a) Array factor of the $2N \times 2M$-element array. (b) Local grating lobe location of $N \times M$-element array.

Chapters/Ch6_Figs/PIC/New/H_pol_2x34_CFGA1.pdf

(a)

Chapters/Ch6_Figs/PIC/New/H_pol_2x34_CFGA2.pdf

(b)

Figure 7: Comparison of the horizontal polarization radiation pattern of a $2 \times 34$-element array with normal configuration calculated with two methods. (a) $2 \times 2$-element array pattern; (b) $2 \times 34$-element array radiation pattern.

Chapters/Ch6_Figs/PIC/New/V_pol_2x34_CFGA1.pdf

(a)

Chapters/Ch6_Figs/PIC/New/V_pol_2x34_CFGA2.pdf

(b)

Figure 8: Comparison of the vertical polarization radiation pattern of a $2 \times 34$-element array with normal configuration calculated with two methods. (a) $2 \times 2$-element array pattern; (b) $2 \times 34$-element array radiation pattern.

Chapters/Ch6_Figs/PIC/New/CFGA_2x6_2x341.pdf

(a)

Chapters/Ch6_Figs/PIC/New/CFGA_2x6_2x342.pdf

(b)

Figure 9: Simulated radiation pattern of the $2 \times 2$-element subarray of a probe-fed patch antenna with configuration ”A”; (a) embedded $2 \times 2$-element pattern, (b) $2 \times 34$-element array pattern.

Chapters/Ch6_Figs/PIC/New/CFGA_2x6_2x34_2n1.pdf Chapters/Ch6_Figs/PIC/New/CFGA_2x6_2x34_2n2.pd

(a) (b)

Figure 10: Simulated radiation pattern of the $2 \times 2$-element subarray of a probe-fed patch antenna with configuration "A"; (a) embedded $2 \times 2$-element patterns of arrays with different number of subarrays, (b) $2 \times 34$-element array patterns.

Chapters/Ch6_Figs/PIC/New/Full_wave_vs_Predicted_C1.pdf Chapters/Ch6_Figs/PIC/New/Full_wave_vs_Predict

(a) (b)

Figure 11: Predicted and full-wave simulated radation pattern of $2\times34$-element array of a probe-fed patch antenna with configuration "C"; (a) H-pol, (b) V-pol.

Chapters/Ch6_Figs/PIC/New/Full_wave_vs_Predicted_PGC1.pdf

(a)

Chapters/Ch6_Figs/PIC/New/Full_wave_vs_Predict

(b)

Figure 12: Predicted and full-wave simulated radation pattern of 2×34-element array of a probe-fed patch antenna with configuration "D"; (a) H-pol, (b) V-pol.

Chapters/Ch6_Figs/PIC/NEW/array_factor.pdf

Figure 13: Array factor of an array of identical subarrays with different element spacings.

Chapters/Ch6_Figs/PIC/New/MPAR_CFG_C_551.pdf

(a)

Chapters/Ch6_Figs/PIC/New/MPAR_CFG_C_552.pdf

(b)

Figure 14: Co and cross-polarization radiation pattern of the $2 \times 130$-element array of the designed single element with configuration "C" at broadside (subarray spacing = 110 mm). (a) Horizontal polarization; (b) Vertical polarization.

Chapters/Ch6_Figs/PIC/New/MPAR_CFG_C_521.pdf

(a)

Chapters/Ch6_Figs/PIC/New/MPAR_CFG_C_522.pdf

(b)

Figure 15: Co and cross-polarization radiation pattern of the $2 \times 136$-element array of the designed single element with configuration "C" at broadside (subarray spacing = 104 mm). (a) Horizontal polarization; (b) Vertical polarization.

Chapters/Ch6_Figs/PIC/New/CFG_C_52_S1.pdf

(a)

Chapters/Ch6_Figs/PIC/New/CFG_C_52_S2.pdf

(b)

Figure 16: Co and cross-polarization radiation pattern of the $2 \times 136$-element array of the designed single element with configuration "C" at broadside (subarray spacing = 104 mm). (a) Horizontal polarization; (b) Vertical polarization.